iScience

CellPress
OPEN ACCESS

Article

The optineurin/TIA1 pathway inhibits aberrant stress granule formation and reduces ubiquitinated TDP-43

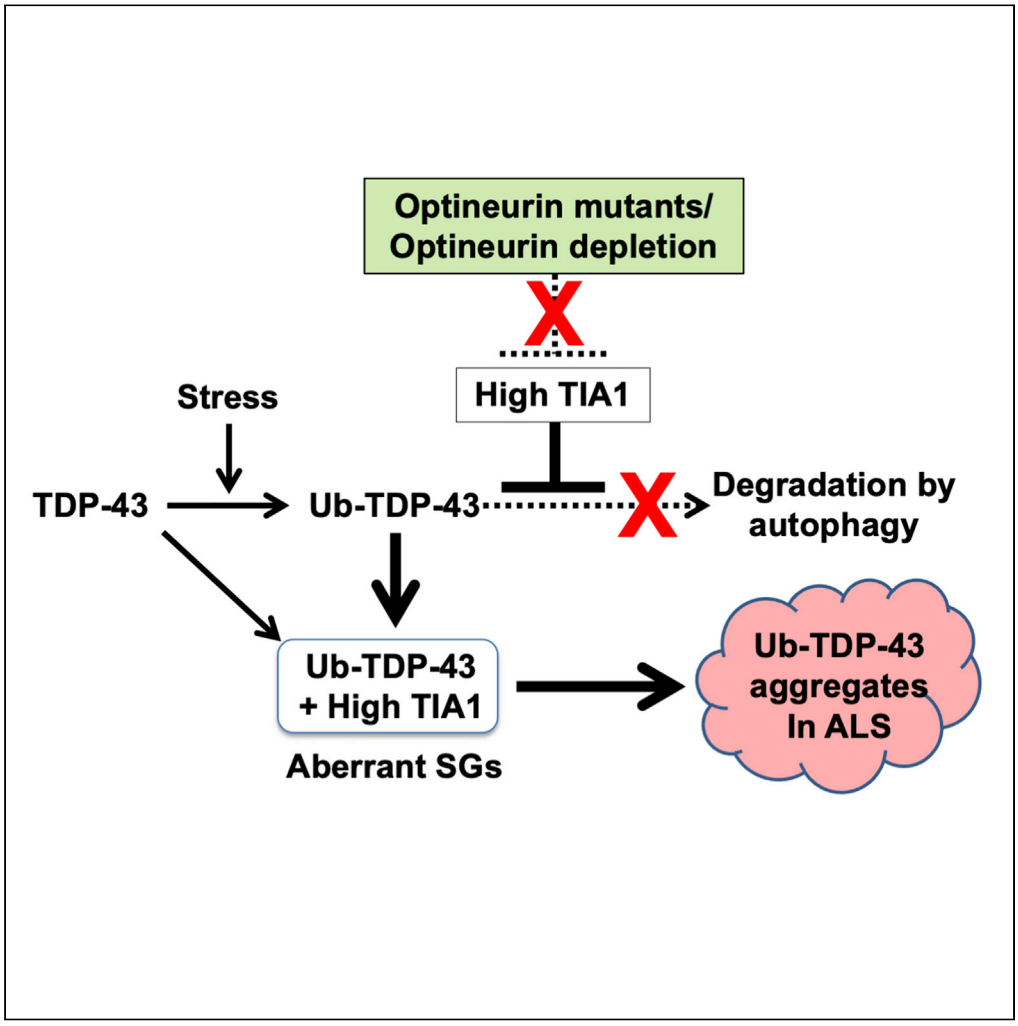

Taichi Kakihana, Masahiko Takahashi, Yoshinori Katsuragi, ..., Tomotake Kanki, Osamu Onodera, Masahiro Fujii

fujiimas@med.niigata-u.ac.jp

Highlights

ALS-linked mutations of optineurin (OPTN) delay clearance of stress granules (SGs).

Depletion of OPTN increases ubiquitinated TDP-43 levels by increasing TIA1

ALS-linked OPTN mutants increase ubiquitinated TDP-43 levels by increasing TIA1

High TIA1 induces aberrant SGs with ubiquitinated TDP-43 and delays SG clearance

Kakihana et al., iScience 24, 102733
July 23, 2021 © 2021
https://doi.org/10.1016/j.isci.2021.102733

iScience

CellPress
OPEN ACCESS

Article

The optineurin/TIA1 pathway inhibits aberrant stress granule formation and reduces ubiquitinated TDP-43

Taichi Kakihana,[1] Masahiko Takahashi,[1] Yoshinori Katsuragi,[1] Shun-Ichi Yamashita,[2] Junya Sango,[1] Tomotake Kanki,[2] Osamu Onodera,[3] and Masahiro Fujii[1,4,*]

SUMMARY

Amyotrophic lateral sclerosis (ALS) is a degenerative motor neuron disease characterized by the formation of cytoplasmic ubiquitinated TDP-43 protein aggregates in motor neurons. Stress granules (SGs) are stress-induced cytoplasmic protein aggregates containing various neuropathogenic proteins, including TDP-43. Several studies have suggested that SGs are the initial site of the formation of pathogenic ubiquitinated TDP-43 aggregates in ALS neurons. Mutations in the *optineurin* (*OPTN*) and *TIA1* genes are causative factors of familial ALS with TDP-43 aggregation pathology. We found that both OPTN depletion and ALS-associated OPTN mutations upregulated the TIA1 level in cells recovered from heat shock, and this upregulated TIA1 increased the amount of ubiquitinated TDP-43. Ubiquitinated TDP-43 induced by OPTN depletion was localized in SGs. Our study suggests that ALS-associated loss-of-function mutants of OPTN increase the amount of ubiquitinated TDP-43 in neurons by increasing the expression of TIA1, thereby promoting the aggregation of ubiquitinated TDP-43.

INTRODUCTION

Various stresses, such as oxidative stress and heat stress, induce protein aggregates called stress granules (SGs) in the cytoplasm of many cell types (Corbet and Parker, 2020; Kedersha et al., 1999). SGs are stress-induced protein aggregates, but these aggregates are cleared as the level of stress decreases. However, a growing body of evidence suggests that SGs initiate the aggregation of pathogenic proteins, which is a key factor for the development of various neurodegenerative diseases, including amyotrophic lateral sclerosis (ALS) (Advani and Ivanov, 2020; Ganassi et al., 2016; Mateju et al., 2017; Molliex et al., 2015; Verdile et al., 2019).

ALS is a fatal motor neuron disease characterized by the loss of upper and lower motor neurons (Masrori and Van Damme, 2020). More than 25 genes have been identified as causative factors of familial and sporadic ALS (Ito et al., 2017). Among them, TAR DNA-binding protein 43 (TDP-43) is a key causative factor of ALS with and without TDP-43 mutation (Sreedharan et al., 2008; Yokoseki et al., 2008). TDP-43 forms cytoplasmic protein aggregates in ALS neurons (Arai et al., 2006; Neumann et al., 2006). These cytoplasmic TDP-43 aggregates are toxic to motor neurons and play a central role in the pathogenesis of ALS.

TDP-43 is an RNA-binding protein (RBP) that is primarily localized in the nucleus of basal-state neurons, whereas TDP-43 is localized in cytoplasmic SGs under various stress conditions. Several studies have proposed an intriguing hypothesis, namely that aberrant SGs serve as initiation sites for the pathogenic aggregation of TDP-43 in ALS neurons (Molliex et al., 2015). Aberrant SGs and normal SGs have a significant difference that initiates the pathogenic aggregation of TDP-43. Aberrant SGs show slower clearance kinetics than normal SGs, which stimulates the formation of irreversible TDP-43 protein aggregates (Ganassi et al., 2016; Higashi et al., 2013; Mateju et al., 2017). However, the mechanism responsible for maintaining SG integrity in normal cells while it is abolished in ALS neurons is unclear.

TIA1 mutations are another causative agent of familial ALS (Mackenzie et al., 2017). TIA1 is an RBP with a prion-like domain and is localized to SGs. ALS-associated TIA1 mutations enhance the formation of SGs in cultured neuronal cells (Mackenzie et al., 2017; Wang et al., 2019). These TIA1-induced SGs show delayed

[1]Division of Virology, Niigata University Graduate School of Medical and Dental Sciences, Niigata 951-8510, Japan

[2]Department of Cellular Physiology, Niigata University Graduate School of Medical and Dental Sciences, Niigata 951-8510, Japan

[3]Department of Neurology, Brain Research Institute, Niigata University, Niigata 951-8585, Japan

[4]Lead contact

*Correspondence: fujiimas@med.niigata-u.ac.jp

https://doi.org/10.1016/j.isci.2021.102733

SG clearance. Therefore, ALS-associated pathogenic TIA1 mutations might induce irreversible TDP-43 aggregates in ALS neurons through aberrant SGs formation (Mackenzie et al., 2017; Wang et al., 2019).

Optineurin (OPTN) is another causative protein of familial ALS (Maruyama et al., 2010). ALS patients with OPTN mutation possess cytoplasmic TDP-43 inclusion bodies in their motor neurons. OPTN has many functions (Markovinovic et al., 2017). For example, OPTN is a ubiquitin receptor that regulates autophagy (Wild et al., 2011). OPTN inhibits the transcription of genes regulated by transcription factor NF-κB (Zhu et al., 2007).

In this study, we investigated the function of OPTN in aberrant SG formation. We found that both OPTN depletion and ALS-associated pathogenic OPTN mutations induce aberrant SGs containing large amounts of ubiquitinated TDP-43 in cultured cells, which is mediated by the upregulation of the expression of TIA1. Therefore, this study suggests that the OPTN/TIA1 pathway is a key system that inhibits neuropathogenic aberrant SG formation, thereby protecting the neuropathogenic aggregation of TDP-43 in ALS motor neurons.

RESULTS

OPTN depletion alters SG phenotype

OPTN is a causative factor of familial ALS with TDP-43 aggregation pathology in motor neurons (Maruyama et al., 2010). Accumulating evidence suggests that SGs initiate the pathogenic aggregation of TDP-43 in ALS neurons (Advani and Ivanov, 2020). To investigate the function of OPTN in normal and/or aberrant SG formation, we examined whether OPTN is localized in SGs induced by heat shock in cultured cells. HeLa cells were exposed to heat shock at 44°C for 30 min and immunostained with anti-OPTN and anti-TIA1 (a marker for SG) antibodies (Figure 1A). In the basal state, OPTN was localized mainly in the cytoplasm. Heat shock-nduced numerous TIA1-positive SGs in the cytoplasm. These SGs were not colocalized with OPTN, indicating that OPTN is not a component of SGs.

To investigate whether the depletion of OPTN alters SG formation, HeLa cells were transfected with *OPTN*-specific small interfering RNA (siRNA) (OPTN-knockdown, OPTN-KD) or control siRNA (*NT*) and exposed to heat shock (Figures 1B and S1A). OPTN-KD doubled the size of SGs in comparison to control (Figures 1C–1D). These results suggested that OPTN reduces the size of SGs in HeLa cells.

SG disappears after the level of stress decreases (Kedersha et al., 1999). Importantly, delayed SG clearance is characteristic of aberrant SGs that induce ubiquitinated TDP-43 aggregates in neuronal cells (Li et al., 2013; Suk and Rousseaux, 2020). We therefore investigated whether OPTN-KD affects the clearance of SGs. OPTN-KD cells were exposed to heat shock at 44°C for 30 min, and further incubated at 37°C for 1 h to recover from stress, and cells were then immunostained with anti-G3BP1 (another SG marker) and anti-TIA1 antibodies. SGs were detected in approximately 90% of OPTN-KD cells after recovery, and the level was significantly higher than that in control cells (approximately 30%) (Figures 1E, 1F, S1A, and S1B). Such delayed SG clearance was also observed in *OPTN*-knockout (OPTN-KO) HeLa cells established by the CRISPR/Cas9-mediated method (Figures S2A and S2B). Sodium arsenite treatment of various types of cells has been shown to induce SG formation (Kedersha et al., 1999). Clearance of SG induced by arsenite was significantly delayed in OPTN-KD cells compared to control cells (Figures S3A and S3B). We also investigated the OPTN activity on SG clearance in Neuro-2a, a mouse neuronal cell line. Neuro-2a cells were transfected with *OPTN-siRNA* and treated with MG-132 (a proteasome inhibitor). SG formation has been reported to be induced by MG-132 treatment and then reduced by prolonged treatment (Ganassi et al., 2016). At 4 h after MG-132 treatment, SGs were detected in approximately 40% of OPTN-KD cells, which was comparable to that of control cells. After 8 h of MG-132 treatment, more OPTN-KD cells carried SGs than control cells (18.3-19% versus 5.5%) (Figures S2D–S2F). To examine the role of OPTN in SG formation in primary neurons, human-induced pluripotent cells (iPSCs) were differentiated into neurons as describe previously (Figures 2A and 2B) (Soeda et al., 2019). The differentiated iPSC-derived cells expressed the neuronal marker protein MAP-2 and TUJ-1 (Figures 2B and 2F). OPTN-KD in iPSC-derived neurons significantly delayed SG clearance after heat shock and recovery (Figures 2C and 2D). These results suggested that OPTN promotes the clearance of SGs in HeLa, Neuro-2a, and iPSC-derived primary neurons, induced by three types of stresses (heat shock, sodium arsenite, and proteasome inhibitor). In addition, OPTN-KD increased the size of SGs in iPSC-derived neurons (Figures 2C and 2E), but the increase in SGs size by OPTN-KD was smaller than that in HeLa cells (Figures 1D and 2E). The size of SGs is determined

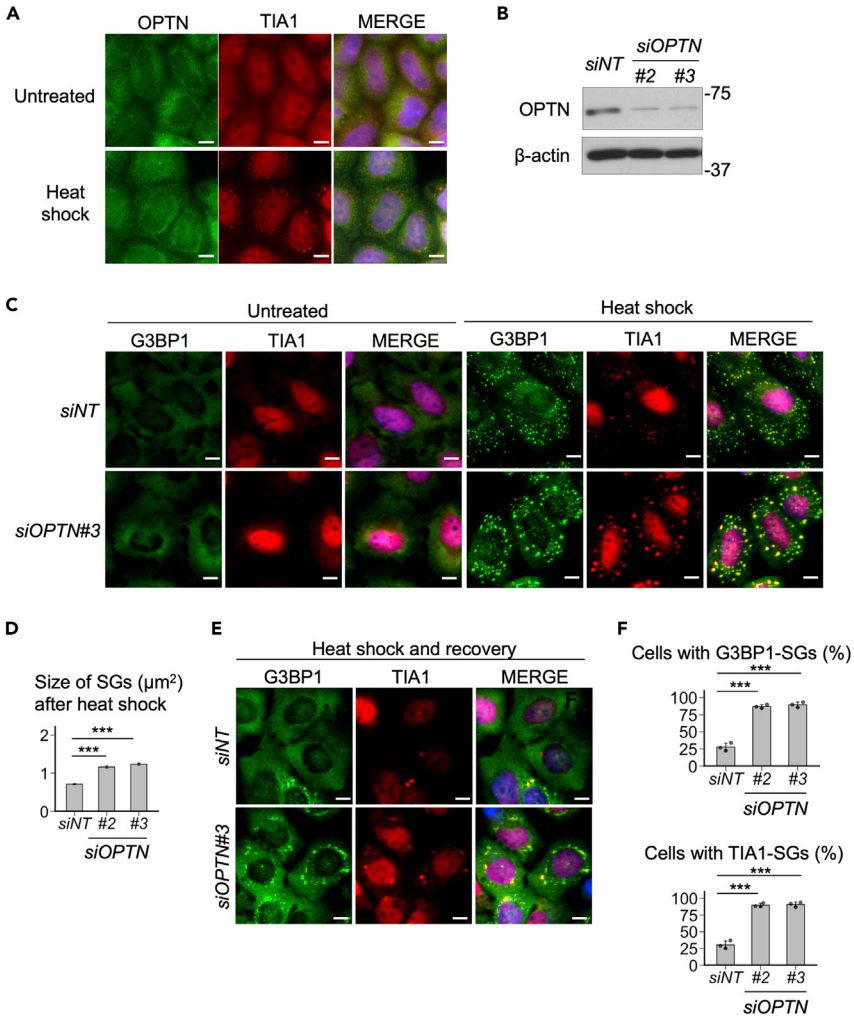

Figure 1. OPTN controls the size of SGs and clearance after heat shock in HeLa cells

(A) HeLa cells were exposed to a temperature of 44°C for 30 min. Cells were immunostained with anti-TIA1 and anti-OPTN antibodies.

(B) HeLa cells were transfected with *OPTN-siRNA* (*# 2* or *# 3*) or control (si*NT*) by Lipofectamine RNAiMAX. At 48 h after transfection, the cells were lysed, and cell lysates were analyzed by Western blotting with the indicated antibodies.

(C–F). HeLa cells were transfected with *OPTN-siRNA* (*# 2* or *# 3*) or control (si*NT*) with Lipofectamine RNAiMAX. At 48 h after transfection, cells were exposed to a temperature of 44°C for 30 min and allowed to recover at 37°C for 60 min. Cells were immunostained with anti-G3BP1 and anti-TIA1 antibodies. Images were obtained by fluorescence microscopy in (C and E), and the sizes of SGs in (D) were measured by the FIJI ImageJ software program. The data are presented as the means ± standard error (SE) ($n > 1000$). The population (%) of cells with either G3BP1-SG or TIA1-SG after recovery is shown in (F). The data are presented as the means ± SD ($n = 3$). ***$p < 0.001$ by one-way analysis of variance (ANOVA) with a Tukey post hoc test. Scale bar indicates 10 μm.

See also Figures S1–S3.

by the total amount of all SG proteins, including TIA1. Therefore, these results suggest that the relative abundance of TIA1 in SGs in iPSC-derived neurons is smaller than that of HeLa cells.

OPTN-KD increases the expression of TIA1

To address how OPTN regulates the formation and clearance of SGs, we measured the expression levels of three SG component proteins (G3BP1, TIA1 and USP10) in OPTN-KD cells. OPTN-KD increased TIA1 level in HeLa cells in the basal state but had little effect on G3BP1 and USP10 levels (Figures 3A and 3B). TIA1 level was also increased in OPTN-KO cells and iPSC-derived primary neurons (Figures 2C and 2F). These

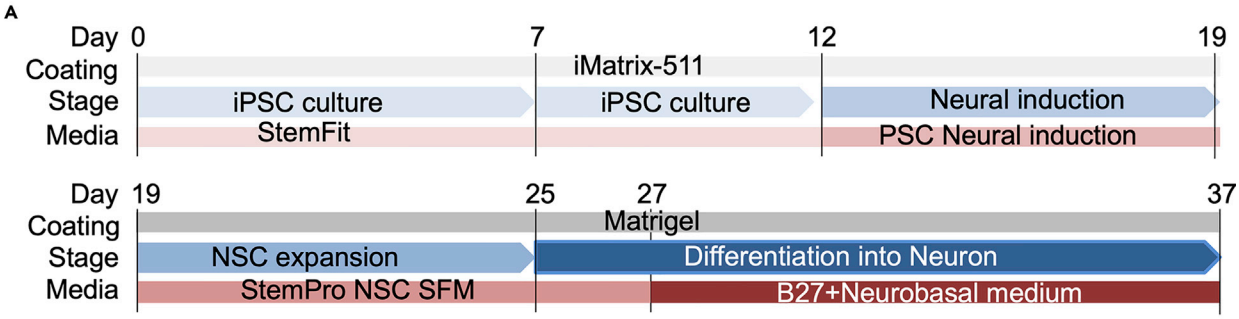
A
Day 0
7
12
19
Coating
iMatrix-511
Stage
iPSC culture
iPSC culture
Neural induction
Media
StemFit
PSC Neural induction
Day 19
25
27
37
Coating
Matrigel
Stage
NSC expansion
Differentiation into Neuron
Media
StemPro NSC SFM
B27+Neurobasal medium

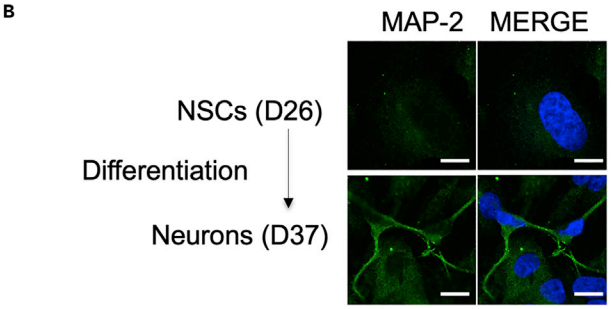
B
MAP-2
MERGE
NSCs (D26)
Differentiation
Neurons (D37)

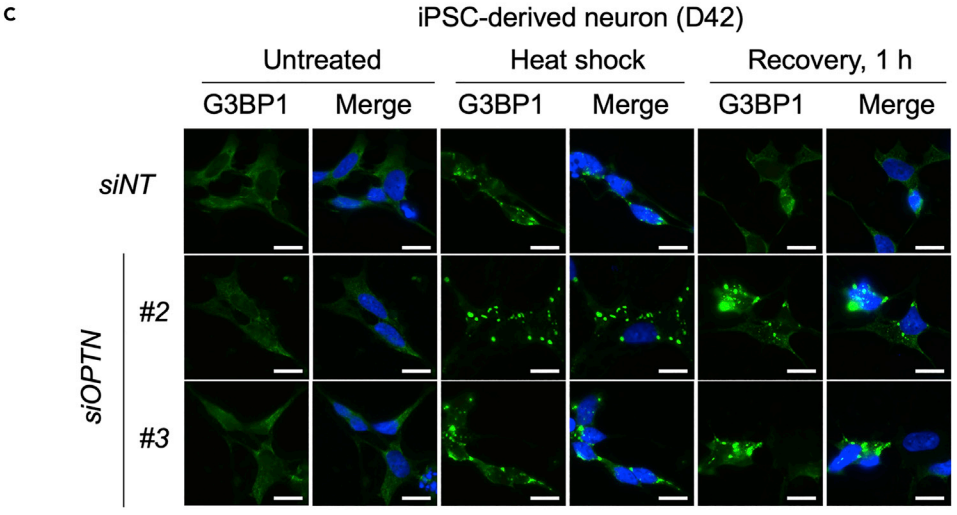
C
iPSC-derived neuron (D42)
Untreated
Heat shock
Recovery, 1 h
G3BP1
Merge
G3BP1
Merge
G3BP1
Merge
siNT
siOPTN
#2
#3

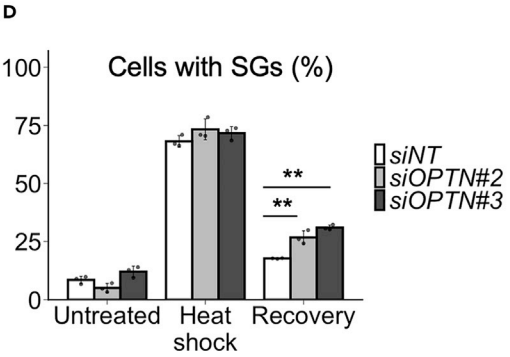
D
Cells with SGs (%)
100
75
50
25
0
**
**
siNT
siOPTN#2
siOPTN#3
Untreated
Heat shock
Recovery

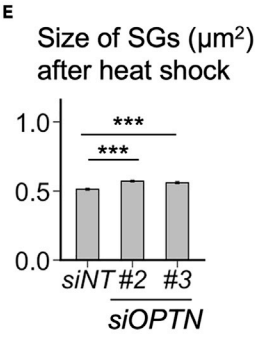
E
Size of SGs (μm²) after heat shock
1.0
0.5
0.0
***
***
siNT
#2
#3
siOPTN

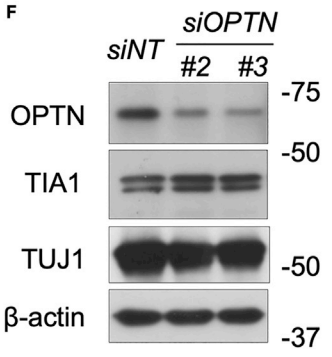
F
siNT
siOPTN
#2
#3
OPTN
TIA1
TUJ1
β-actin
-75
-50
-50
-37

Figure 2. OPTN-KD delays clearance of heat shock-induced SGs in iPSC-derived neurons

(A) Schematic representation of the differentiation protocols from iPSCs to neural stem cells (NSCs, days 12-25) and from NSCs to neurons (days 25-37).

(B) Immunostaining of NSCs (days 26, D26) and neurons (D37) with anti-MAP-2 antibody and Hoechst 288381, Images were obtained by fluorescence microscopy.

(C–F) iPSC-derived neurons (days 38) were transfected with *OPTN-siRNA* (*# 2* or *# 3*) or control (*siNT*) with Lipofectamine RNAiMAX. At 72 h after transfection, cells were exposed to a temperature of 44°C for 30 min and incubated at 37°C for 1 h to recover from stress. Cells were then immunostained with anti-G3BP1 antibody. Images were obtained by fluorescence microscopy in (C), and the population (%) of cells with G3BP1-SG after recovery in (D) and the size of SGs in (E) were measured by the CellProfiler software program. The population (%) of cells with G3BP1-SG after recovery (D) are presented as the means ± SD (n = 3). The sizes of SGs in (E) are presented as the means ± SE (n > 1000). *p < 0.05, ***p < 0.001 by one-way ANOVA with a Tukey post hoc test. Scale bar indicates 10 μm. Cell lysates were analyzed by Western blotting using the indicated antibodies in (F).

results suggested that the enhanced expression of TIA1 in OPTN-KD cells might alter SG-related phenotypes.

OPTN has been reported to suppress the gene expression regulated by transcription factor NF-κB (Zhu et al., 2007). Thus, we next investigated whether OPTN-KD regulates the expression of *TIA1* mRNA. OPTN-KD increased the amount of *TIA1* mRNA, and the increase was hardly affected by NF-κB inhibitor (BAY-11-7082) treatment (Figure 3C). These results suggest that OPTN-KD induces the expression of *TIA1* at the mRNA level in an NF-κB-independent manner.

Previous reports indicate that OPTN enhances selective autophagy. For instance, OPTN functions as an autophagy receptor for damaged mitochondria in mitochondrial autophagy (also called mitophagy) (Wong and Holzbaur, 2014). We therefore investigated whether OPTN-KD increases TIA1 protein levels by inhibiting autophagy or proteasome-mediated degradation. Treatment with a proteasome inhibitor (MG-132) or autophagy inhibitor (bafilomycin A1, Baf) had little effect on the TIA1 protein levels in OPTN-KD cells (Figure 3D). These results suggested that neither autophagy nor proteasomes play a major role in increasing the TIA1 protein level in OPTN-KD cells.

Autophagy has been shown to promote SG clearance (Buchan et al., 2013). To determine whether or not autophagy is involved in the regulation of SG clearance by OPTN, we investigated whether or not OPTN-KD delays SG clearance in autophagy-defective cells. ATG7 induces LC3 lipidation (LC3-II formation), which is required for autophagosome formation (Figure 3E). We transfected *OPTN-siRNA* into ATG7-KO cells and then characterized cells for their SG clearance after heat shock. OPTN-KD induced a delay in SG clearance in autophagy-deficient ATG7-KO cells (Figures 3F and 3G). These results suggest that OPTN-KD delays SG clearance in an autophagy-independent mechanism (Figures 3F–3H). In addition, OPTN-KD increased the size of SGs in ATG7-KO cells (Figure 3H), but the increase was smaller than that in parental ATG7-WT cells (Figures 1D and 3H). These results suggest that OPTN suppresses the size of SGs by both autophagy-dependent and autophagy-independent mechanisms.

TIA1-KD attenuates a delay of SG clearance in OPTN-KD cells

Next, we investigated the role of TIA1 in the delay of SG clearance in OPTN-KD cells. OPTN-KD delayed SG clearance in heat shock-treated HeLa cells, but the delay was attenuated by TIA1-KD (Figures 4A–4C). In addition, OPTN-KD increased the size of SGs (Figure 1D), and the size of SGs increased by OPTN-KD was decreased by TIA1-KD (Figures 4D and 4E). These results suggested that OPTN-KD delays SG clearance and increases the size of SGs by promoting the expression of TIA1.

OPTN-KD induces TDP-35/ubiquitin-positive SGs

The formation of cytoplasmic TDP-43 inclusion bodies in motor neurons is a characteristic pathology in patients with ALS, including those with OPTN mutation (Maruyama et al., 2010; Nakazawa et al., 2016). Importantly, accumulating evidence suggests that aberrant SGs serve as the site of initiation for the aggregation of TDP-43 in ALS neurons (Molliex et al., 2015). We therefore investigated whether the depletion of OPTN affects the formation of TDP-43-positive SGs. In the basal state, TDP-43 was primarily localized in the nucleus of both OPTN-KD and control cells (Figure 5A, top). Heat shock treatment reduced nuclear TDP-43 localization and induced cytoplasmic TDP-43-positive SGs (TDP-43-SGs) in OPTN-KD cells, which were more numerous than control cells (Figures 5A and 5B). In addition, after recovery from heat shock, the number of cells with TDP-43-SGs in OPTN-KD cells was greater than that in control cells (Figures 5A and 5B). These results suggest that the depletion of OPTN increases the SG localization of TDP-43 and that the formation of these TDP-43-SGs is further increased during recovery from heat shock. Like heat shock, the

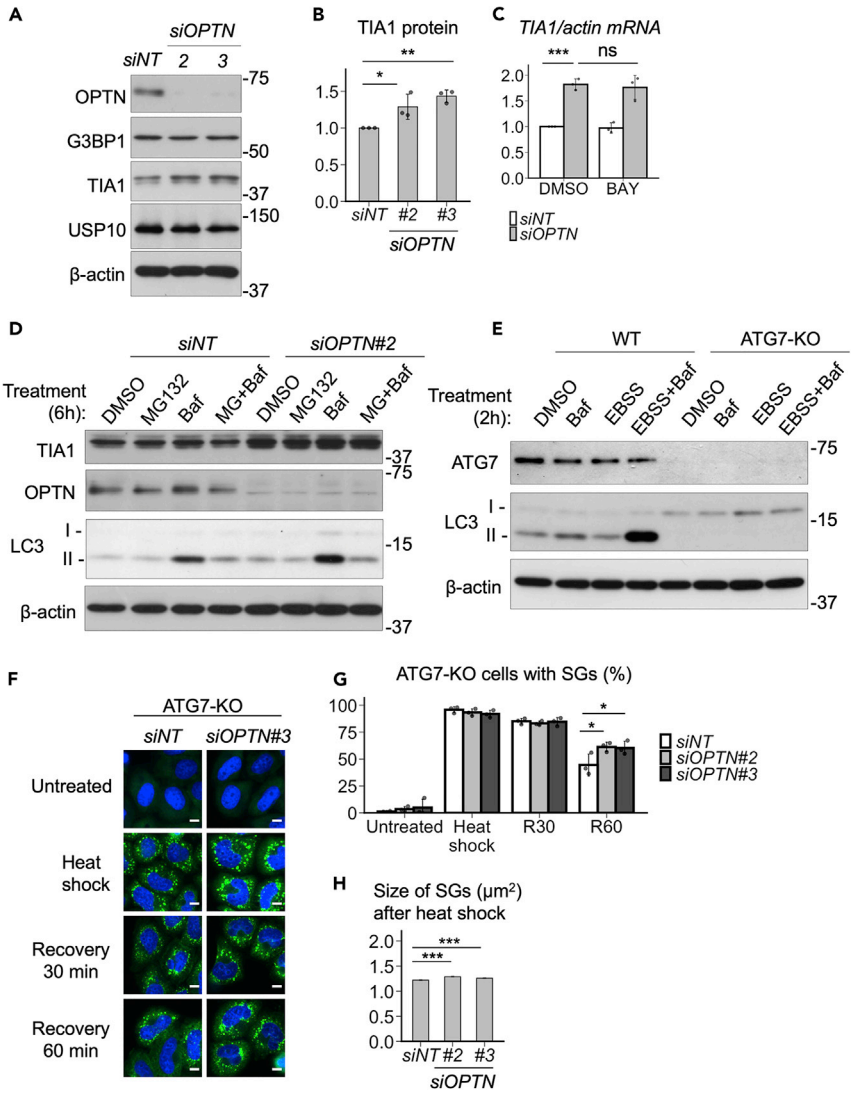

Figure 3. OPTN-KD increases the TIA1 mRNA levels in HeLa cells

(A and B) HeLa cells were transfected with *OPTN-siRNA* (*# 2* or *# 3*) or control (*siNT*) by Lipofectamine RNAiMAX. At 48 h after transfection, cell lysates were analyzed by Western blotting with the indicated antibodies. The amount of TIA1 was measured by densitometry. The ratio of TIA1 band of OPTN-KD cells to controls cells is shown in (B). The data are presented as the means ± SD (n = 3). *p < 0.05, **p < 0.01.

(C) HeLa cells were transfected with *OPTN-siRNA* (*# 2*) or control (*siNT*). At 32 h after transfection, cells were treated with BAY-11-7082 (NF-κB inhibitor) or DMSO for 16 h. Total RNA was extracted from these cells and the relative expression of *TIA1* to *β-actin* was measured by real-time reverse transcription PCR (RT-PCR) using the corresponding primer sets. The data are presented as the means ± SD (n = 3). ***p < 0.001.

(D) HeLa cells were transfected with *OPTN-siRNA* (*# 3*) or control (*siNT*). At 48 h after transfection, cells were treated with 5 μM MG-132 (MG), 50 nM bafilomycin A1 (Baf), their combination (MG + Baf) or DMSO for 6 h. Cell lysates prepared from these cells were characterized by Western blotting using the indicated antibodies.

(E–H) (E) ATG7-KO or control ATG7-WT HeLa cells were cultured in 10% FBS/DMEM for 24 h. Cells were then washed with PBS and further cultured in 10% FBS/DMEM (nutrient-rich medium) or Earle's Balanced Salt Solution (EBSS, nutrient-deficient medium) with 125 nM bafilomycin A1 (Baf) or DMSO for 2 h. Cells were lysed and analyzed by Western blotting with the indicated antibodies. (F and H) ATG7-KO HeLa cells were transfected with *OPTN-siRNA* (# 2 or # 3) or control (*siNT*) with Lipofectamine RNAiMAX. At 48 h after transfection, cells were exposed to a temperature of 44°C for 30 min and incubated at 37°C for 1 h to recover from stress. Cells were immunostained with anti-G3BP1 antibody. Images were obtained by fluorescence microscopy in (F), and the population (%) of cells with G3BP1-SG after recovery in (G), and the size of SGs in (H) were measured by the CellProfiler software program. The population (%) of cells with G3BP1-SG after recovery are presented as the means ± SD (n = 3). The sizes of SGs are presented as the means ± SE (n > 1000). *p < 0.05, ***p < 0.001 by one-way ANOVA with a Tukey post hoc test. Scale bar indicates 10 μm.

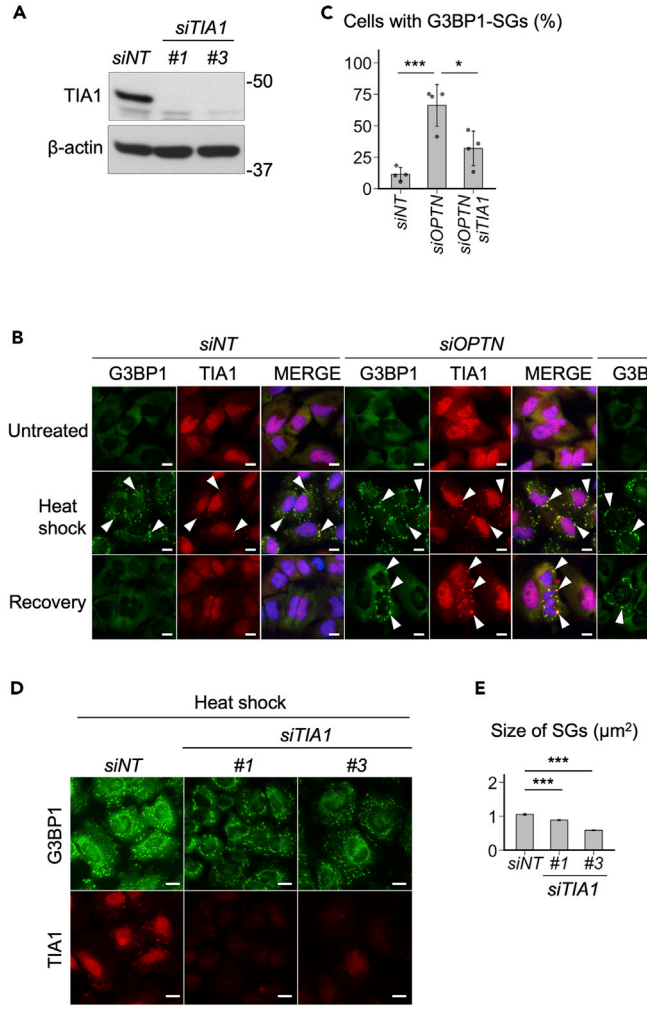

Figure 4. TIA1-KD attenuates the OPTN-KD activity in SGs in HeLa cells

(A) HeLa cells were transfected with *TIA1-siRNA* (*# 1* or *# 3*) or control (*siNT*). At 48 h after transfection, cell lysates were analyzed by Western blotting with the indicated antibodies.

(B and C) HeLa cells were transfected with *OPTN-siRNA* (*# 2*), *OPTN-siRNA* (*# 2*) + *TIA1-siRNA* (*# 1*) or control (*siNT*). At 48 h post-transfection, cells were untreated or exposed to a temperature of 44°C for 30 min and allowed to recover at 37°C for 90 min. Cells were immunostained with anti-G3BP1 and anti-TIA1 antibodies. G3BP1-SG-positive cells (indicated by arrowheads) were measured. The proportion of cells with G3BP1-SG (%) is shown in (C). The data are presented as the means ± SD (n = 4). *$p < 0.05$, ***$p < 0.001$.

(D and E) HeLa cells were transfected with *TIA1-siRNA* (*# 1* or *# 3*) or control (si*NT*). At 48 h after transfection, cells were exposed to a temperature of 44°C for 30 min. Cells were immunostained with anti-G3BP1 and anti-TIA1 antibodies and the SG size of the stained cells was measured using the FIJI ImageJ software program. The data are presented as the means ± SE (N > 1000). ***$p < 0.001$ by one-way ANOVA with a Tukey post hoc test. Scale bar indicates 10 μm.

formation of TDP-43-SG after recovery from sodium arsenite treatment was more strongly detected in OPTN-KD cells than in control OPTN-WT cells (Figures S3A–S3C).

TDP-43 is cleaved to generate a C-terminal fragment TDP-35, which is increased by stress (McGurk et al., 2018; Zhang et al., 2009). Intriguingly, TDP-35 protein is detected in cytoplasmic TDP-43-positive aggregates of ALS motor neurons (Xiao et al., 2015). TDP-43 has a nuclear localization signal (NLS) at the N-terminal part and is primarily localized in the nucleus. On the other hand, TDP-35 lacks NLS, and therefore localizes to both the cytoplasm and nucleus (Li et al., 2015; Zhang et al., 2009). These reports suggest that TDP-35 may play a pathological role in the formation of cytoplasmic TDP-35/TDP-43 aggregates in ALS neurons (Neumann et al., 2006; Wils et al., 2010). GFP-TDP-35 is a fusion protein of TDP-35 and green

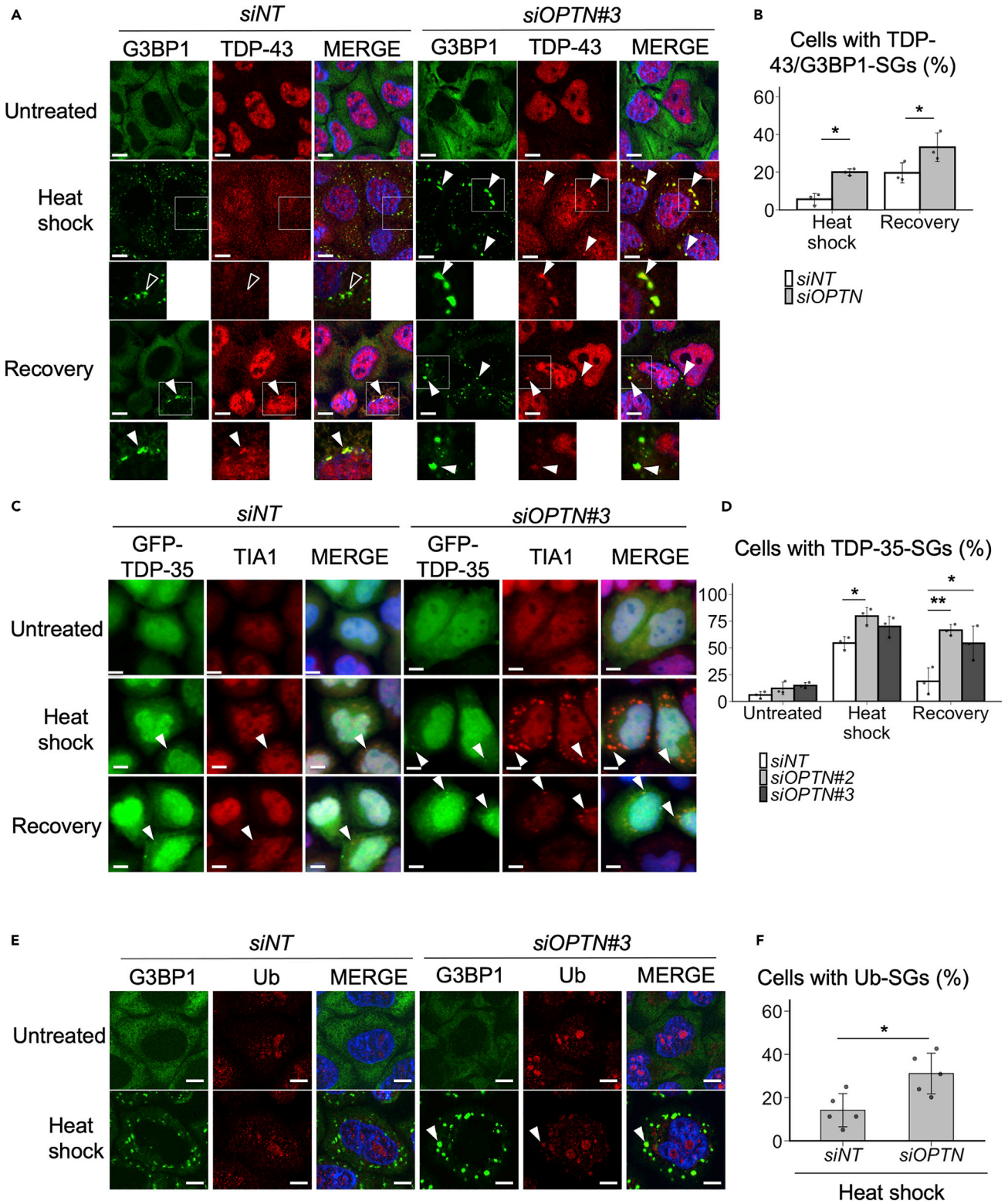

Figure 5. OPTN-KD increases the amount of ubiquitinated TDP-35 and ubiquitin in SGs

(A and B) HeLa cells were transfected with *OPTN-siRNA* (*# 3*) or control (*siNT*). At 48 h after transfection, the cells were untreated or exposed to a temperature of 44°C for 30 min and allowed to recover at 37°C for 60 min. Cells were immunostained with anti-G3BP1 and anti-TDP-43 antibodies. Closed arrowheads

Figure 5. *Continued*

indicate cells with TDP-43-SGs. Open arrowheads indicate cells with TDP-43-negative SGs. The percentage of cells containing TDP-43-SG is shown in (B). The data are presented as the means ± SD (n = 3). *p < 0.05.

(C and D) HeLa cells were transfected with *OPTN-siRNA* (*# 2* or *# 3*) or control (*siNT*). The next day, the cells were transfected with GFP-TDP-35. At 48 h after transfection, cells were untreated or exposed to a temperature of 44°C for 30 min and allowed to recover at 37°C for 45 min. Cells were immunostained with anti-GFP and anti-TIA1 antibodies. Arrowheads indicate cells with TDP-35-SGs. The cells containing TDP-35/TIA1-SG (TDP-35-SG) were counted. The percentage of cells with TDP-35-SG is shown in (D). The data are presented as the means ± SD (n = 3). *p < 0.05, **p < 0.01.

(E and F) HeLa cells were transfected with *OPTN-siRNA* (*# 3*). At 48 h after transfection, cells were untreated or exposed to a temperature 44°C for 30 min. Cells were immunostained with anti-G3BP1 and anti-Ub antibodies. Cells containing Ub/G3BP1-SG (Ub-SG) were counted. The proportion of cells with Ub-SG is shown in (F). The data are presented as the means ± SD (n = 5). *p < 0.05 by one-way ANOVA with a Tukey post hoc test. Scale bar indicates 10 μm.

fluorescent protein (GFP). The overexpression of GFP-TDP-35 induced a small number of GFP-TDP-35/TIA1-positive SGs (TDP-35-SGs) in OPTN-KD and control cells (Figures 5C and 5D). Heat shock-induced TDP-35-SGs in OPTN-KD cells, which was slightly higher than that in control cells. In control cells, the formation of TDP-35-SGs was significantly reduced during the recovery phase, but this reduction was attenuated in OPTN-KD cells. These results suggested that OPTN-KD delays the clearance of TDP-35-positive SGs.

Aberrant SGs contain more ubiquitinated proteins than normal SGs (Ganassi et al., 2016; Mateju et al., 2017). We therefore measured the localization of ubiquitin in SGs in OPTN-KD cells. G3BP1 and ubiquitin double-positive SGs (Ub-SGs) were detected in OPTN-KD cells exposed to heat shock, the number of which is higher than that in control cells (Figures 5E and 5F). These results suggested that OPTN-KD increased the number of ubiquitin-positive SGs in cells exposed to heat shock.

The overexpression of TIA1, but not G3BP1, delays SG clearance

The data above suggested that the increased expression of TIA1 protein induced by OPTN-KD plays a role in aberrant SG formation (Figures 4B and 4C). Therefore, the involvement of TIA1 and G3BP1 in SG clearance was compared by transfecting HeLa cells with FLAG-tagged TIA1 (FLAG-TIA1) or FLAG-tagged G3BP1 (FLAG-G3BP1) plasmid. PABP1 (polyadenylate-binding protein 1) was used as an SG marker protein. The overexpression of FLAG-TIA1 induced PABP1-positive SGs in approximately 8% of HeLa cells, and the SG-positive cell population increased to 100% with heat shock treatment; this level was comparable to that of control and G3BP1-overexpressing cells (Figures 6A and 6B). After 1 h of recovery from heat shock, the overexpression of FLAG-TIA1 but not FLAG-G3BP1 caused a significant delay in SG clearance (Figures 6A and 6B). In contrast to OPTN-WT cells, the overexpression of FLAG-TIA1 in OPTN-KO cells did not delay the clearance of SGs (Figure S4). Given that OPTN-KO delayed SG clearance and simultaneously increases the amount of TIA1 (Figures S2A and S2C), these results suggest that the delay in SG clearance by OPTN-KO was mediated by increased TIA1 expression.

OPTN-KD promoted the recruitment of TDP-43 and ubiquitin in SGs (Figure 5). Next, we investigated the role of the overexpression of TIA1 in recruitment of TDP-43 and ubiquitin to SGs. The overexpression of FLAG-TIA1 induced the localization of TDP-43, TDP-35 and ubiquitin to SGs more than the overexpression of FLAG-G3BP1 (Figures 6C–6F and S5). These results suggested that the increase in TIA1 protein induced by OPTN-KD plays a role in promoting the formation of ubiquitin/TDP-43-positive SGs in OPTN-KD cells.

OPTN-KD increases the amount of ubiquitinated TDP-35

ALS neurons possess ubiquitinated TDP-43 inclusion bodies (Arai et al., 2006; Neumann et al., 2006). Next, six histidine-tagged ubiquitin (His-Ub) were used to measure the ubiquitination of TDP-35 in OPTN-KD cells. OPTN-KD HEK293T cells were co-transfected with GFP-TDP-35 and His-Ub, and the cells were lysed with lysis buffer containing 6 M guanidine. His-Ub-modified proteins were purified on nickel-nitrilotriacetic acid (Ni-NTA) agarose and analyzed by Western blotting. The levels of ubiquitinated TDP-35 protein detected in OPTN-KD cells were higher than those in control cells (Figures 7A and 7B). Since OPTN-KD increased the amount of TIA1, we investigated whether the increased expression of TIA1 also induces the ubiquitination of TDP-43/TDP-35. The overexpression of FLAG-TIA1 in HEK293T cells increased TDP-43/TDP-35 ubiquitination over that of FLAG-G3BP1 (Figures 7C and 7D). These results suggested that OPTN-KD stimulates ubiquitin/TDP-43-positive SG formation, in part by increasing TIA1 expression. In addition, OPTN-KD increased the amount of endogenous TDP-35 but not TDP-43 in cells exposed to heat shock (Figures 7E and 7F). Given that OPTN-KD increases the amount of ubiquitinated TDP-35, these

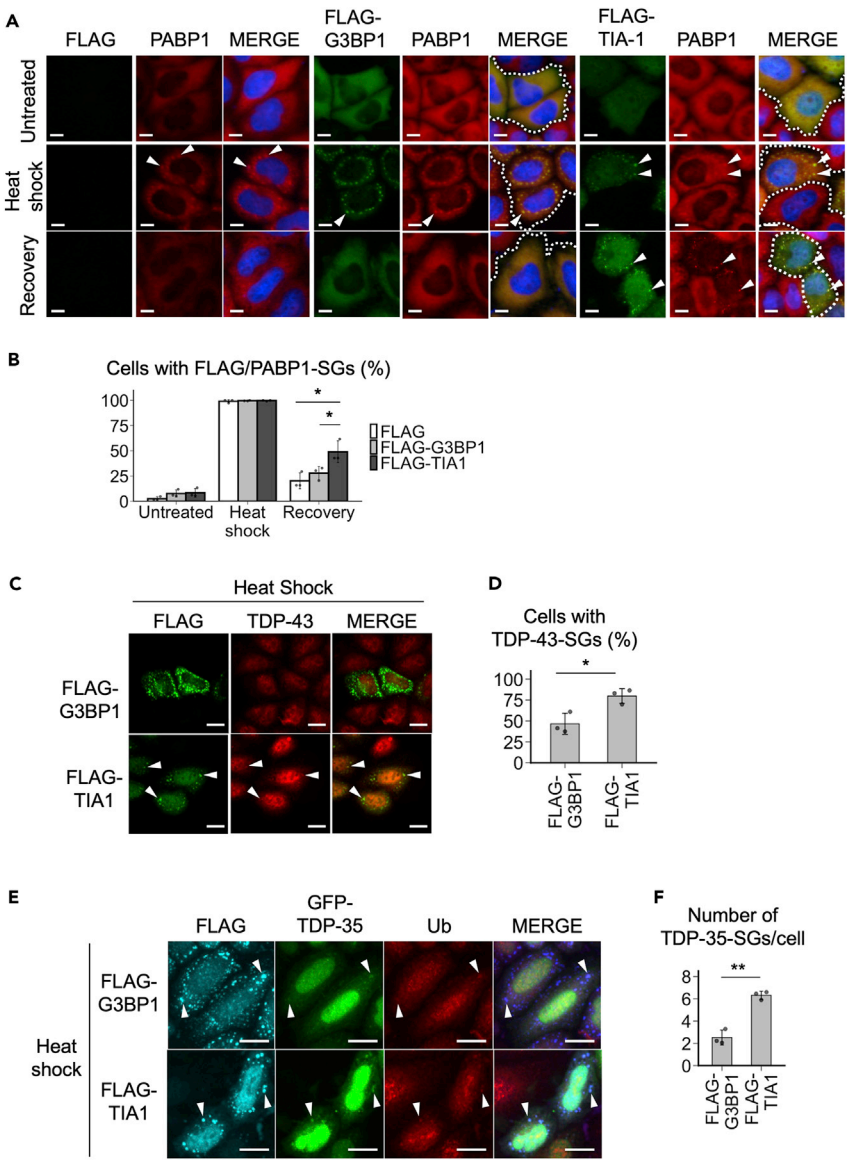

Figure 6. The overexpression of TIA1 but not G3BP1 slows the clearance of SGs

(A and B) HeLa cells were transfected with FLAG-G3BP1, FLAG-TIA1 or control plasmids. At 48 h after transfection, cells were untreated or exposed to a temperature of 44°C for 30 min and allowed to recover at 37°C for 45 min. Cells were immunostained with anti-FLAG and anti-PABP1 antibodies. Cells with FLAG/PABP1-SGs (indicated by arrowheads) were counted. The percentages of cells containing FLAG/PABP1-SG are shown in (B). The data are presented as the means ± SD (n = 3). *p < 0.05.

(C and D) HeLa cells were transfected with FLAG-G3BP1 or FLAG-TIA1 plasmid. At 48 h after transfection, cells were exposed to a temperature of 44°C for 30 min. Cells were immunostained with anti-FLAG and anti-TDP-43 antibodies. Cells with FLAG/TDP-43-SGs (TDP-43-SGs; indicated by arrowheads) were counted. The percentages of cells containing FLAG/TDP-43-SGs (%) are shown in (D). The data are presented as the means ± SD (n = 3). *p < 0.05.

(E and F) HeLa cells were co-transfected with GFP-TDP-35 and FLAG-G3BP1 or FLAG-TIA1 plasmids. At 48 h after transfection, cells were exposed to a temperature of 44°C for 30 min. Cells were immunostained with anti-FLAG antibody. Arrowheads indicate TDP-35-SGs. The number of FLAG/TDP-35-SGs per cell was counted and is shown in (F). The data are presented as the means ± SD (n = 3). **p < 0.01 by one-way ANOVA with a Tukey post hoc test. Scale bar indicates 10 μm.

See also Figures S4 and S5.

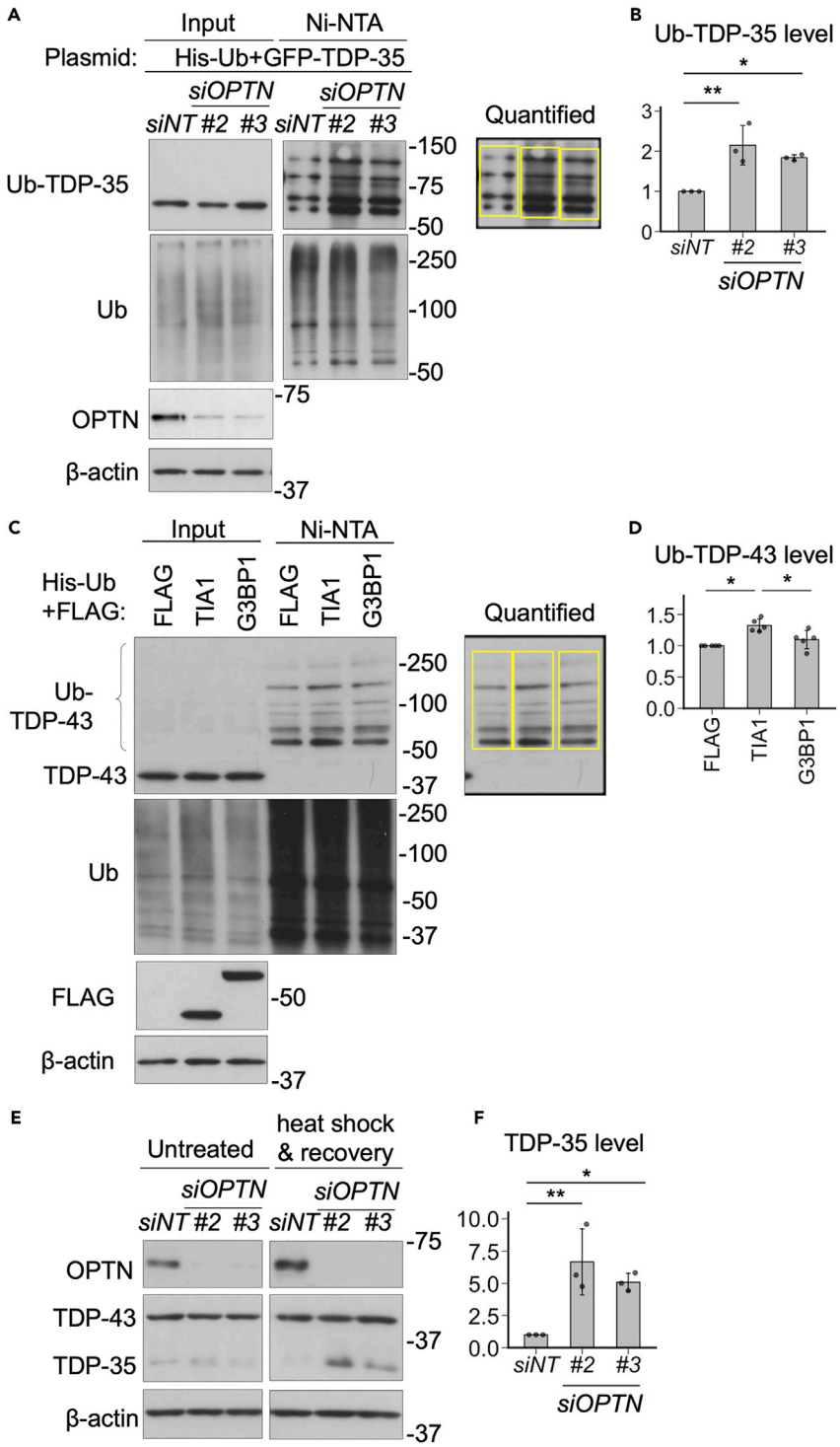

Figure 7. OPTN-KD enhances GFP-TDP-35 ubiquitination

(A and B) HEK293T cells were transfected with *OPTN-siRNA* (*# 2* or *# 3*) or control (*NT*). The next day, cells were co-transfected with GFP-TDP-35 and His-Ub plasmids. At 48 h after transfection, cells were lysed with Buffer A, containing 6 M guanidine, and sonicated. His-Ub-conjugated proteins in cell lysates were purified with Ni-NTA agarose and analyzed by Western blotting with the indicated antibodies. The amount of Ub-GFP-TDP-35 band was measured by densitometry. The ratio of Ub-GFP-TDP-35 band of OPTN-KD cells to control cells is shown in (B). The data are presented as the means ± SD (n = 3). *p < 0.05.

Figure 7. *Continued*

(C and D) HEK293T cells were co-transfected with His-Ub along with FLAG-TIA1 or FLAG-G3BP1 plasmids. At 48 h after transfection, cells were lysed with buffer A, containing 6 M guanidine, and sonicated. His-Ub-conjugated proteins in lysates were purified on Ni-NTA agarose and analyzed by Western blotting with the indicated antibodies. The amount of Ub-TDP band was measured by densitometry. The ratio of Ub-GFP-TDP-35 band of OPTN-KD cells to control cells is shown in (D). The data are presented as the means ± SD (n = 5). *p < 0.05.

(E and F) HeLa cells were transfected with *OPTN-siRNA* (*# 2* or *# 3*) or control (*NT*). At 48 h after transfection, cells were untreated or exposed to a temperature of 44°C for 30 min and allowed to recover at 37°C for 8 h. Cell lysates were analyzed by Western blotting with the indicated antibodies. The amount of ubiquitinated TDP-35 in the cells after heat shock and recovery was measured by densitometry. The ratio of ubiquitinated TDP-35 in OPTN-KD cells in comparison to control cells is shown in (F). The data are presented as the means ± SD (n = 3). *p < 0.05, **p < 0.01 by one-way ANOVA with a Tukey post hoc test.

results suggested that OPTN-KD inhibits the degradation of ubiquitinated TDP-35 in stressed HEK293T cells.

ALS-associated OPTN mutants induce the formation of aberrant SGs containing high levels of TDP-43

Approximately 20 missense OPTN mutations have been identified from familial and sporadic ALS patients (Markovinovic et al., 2017). OPTN has 4 domains; coiled-coil 1 (CC1), CC2, Ub-binding domain in ABIN proteins and NEMO (UBAN), and zinc finger (ZF) domains (Figure 8A). These OPTN mutations have been found in all four domains or in close proximity to these domains. We constructed seven OPTN mutants (K59N, A93P, R96L, V295F, E478G, R545Q, and K557T) with the synonymous mutations resistant to *OPTN-siRNA*, transfected them into OPTN-KD cells, and investigated four aberrant SG-related phenotypes: delayed SG clearance, TIA1 upregulation, increased recruitment of TDP-43 within SGs and increased ubiquitination of TDP-35. While OPTN-KD induced delayed SG clearance in HeLa cells, the delay was attenuated by the expression of OPTN wild-type (OPTN-WT). On the other hand, the expression of five OPTN mutants (K59N, A93P, R96L, E478G, and K557T) hardly rescued the delayed SG clearance phenotype (Figure 8B). In addition, the expression of two OPTN mutants (V295F and R545Q) partially rescued delayed SG clearance. Next, we investigated the effects of OPTN mutants on the expression of TIA1. OPTN-KD increased the amount of *TIA1* mRNA (Figure 3C). While OPTN-WT reduced the amount of *TIA1* mRNA in OPTN-KD cells, six of seven ALS-associated OPTN mutants failed to reduce the expression of *TIA1* mRNA (Figure 8C). In addition, R545Q mutant partially reduced the expression of *TIA1* mRNA. Like *TIA1* mRNA, seven ALS-associated OPTN mutants upregulated the expression of TIA1 protein (Figures S6A and S6B). Third, we investigated the activity of OPTN mutants in the prevention of TDP-43 localization to SGs. OPTN-KD enhanced the localization of TDP-43 to SGs (Figure 5). While the expression of OPTN-WT reduced TDP-43 localization to SGs, six of seven OPTN mutants failed to reduce the localization of TDP-43 to SGs (Figure 8D). Finally, we investigated the activity of OPTN mutants in the ubiquitination of TDP-35. OPTN-KD increased the amount of Ub-TDP-35 in cells treated with proteasome inhibitor (MG-132), but the increase was canceled by the expression of OPTN-WT (Figures 8E and 8F). Unlike OPTN-WT, seven ALS-associated OPTN mutants either increased or slightly decreased the amount of Ub-TDP-35. Furthermore, the increases in the amounts of Ub-TDP-35 by OPTN mutants were reduced by TIA1-KD (Figures 8E and 8F). These results indicate that ALS-associated OPTN mutants are unable to reduce the amount of Ub-TDP-35 and that this defect is mediated by the upregulation of TIA1 by OPTN mutants. Taken together, these results suggested that like OPTN-KD, five of seven ALS-associated OPTN mutants (K59N, A93P, R96L, E478G, and K557T) induce aberrant SG phenotypes (delayed SG clearance, TIA1 upregulation, increased recruitment of TDP-43 in SGs, and increased ubiquitination of TDP-35) and the other two mutants partially induced aberrant SG-related phenotypes.

DISCUSSION

The aggregation of ubiquitinated TDP-43 in motor neurons is the hallmark pathology of ALS with and without OPTN mutations (Ito et al., 2017; Nakazawa et al., 2016). Accumulating evidence suggests that the pathogenic aggregation of TDP-43 in ALS neurons is initiated within aberrant SGs (Maharana et al., 2018; Mateju et al., 2017; Molliex et al., 2015). We found that both OPTN depletion and the overexpression of some ALS-associated OPTN mutants induce aberrant SGs with delayed SG clearance (Figures 1E, 1F, and 8B), increase localization of TDP-43 in SGs (Figures 5 and 8D) and increase ubiquitination of TDP-35/TDP-43 (Figures 7A, 7B, 8E, and 8F). Thus, these findings suggest that OPTN reduces the accumulation of ubiquitinated TDP-43 aggregates by suppressing the formation of aberrant SGs under stress conditions,

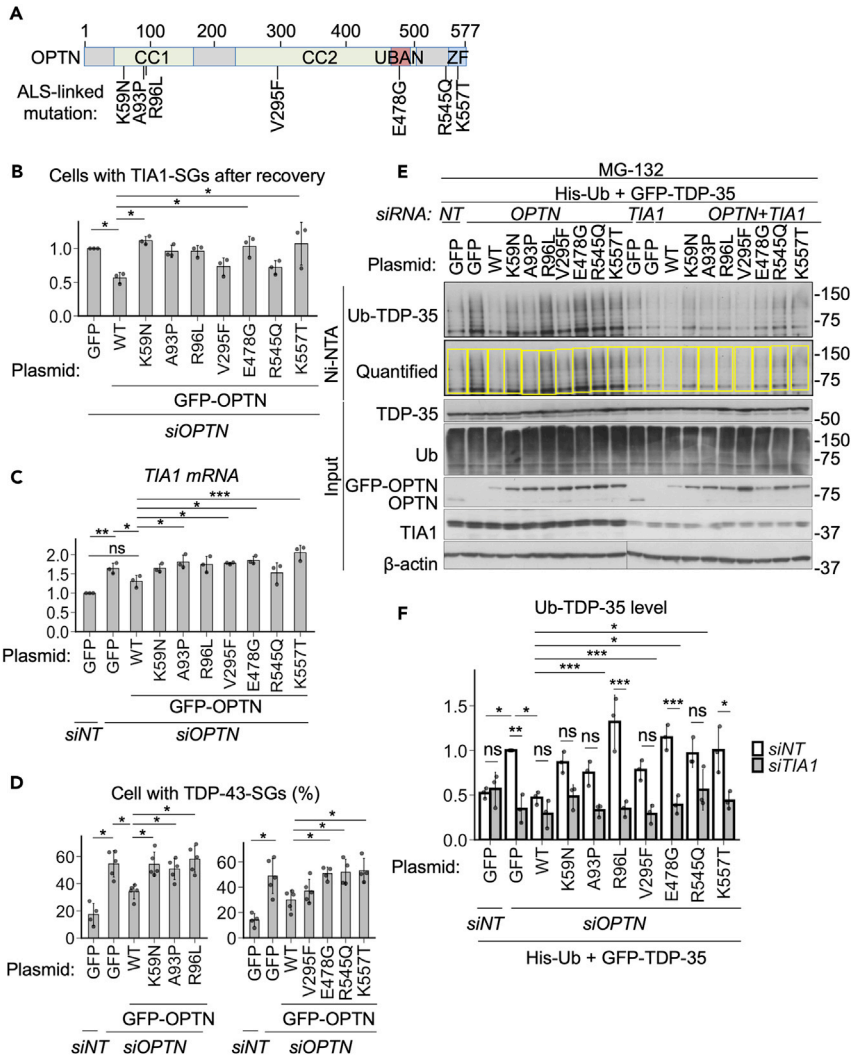

Figure 8. ALS-associated OPTN mutants induce the formation of aberrant SGs containing high levels of TDP-43

(A) Location of ALS-associated mutations in the OPTN amino acid sequence.

(B) HeLa cells were transfected with *OPTN-siRNA* (*# 2*). The next day, cells were transfected with the GFP-OPTN-WT (WT), GFP-OPTN mutant, or control (GFP). At 48 h after transfection, cells were exposed to a temperature of 44°C for 30 min and allowed to recover at 37°C for 60 min. Cells were immunostained with anti-TIA1 antibody. GFP-transfected cells containing TIA1-SG were counted. The data are presented as the means ± SD (n = 3). *p < 0.05.

(C) HEK293T cells were transfected with *OPTN-siRNA* (*# 2*). The next day, cells were transfected with the GFP-OPTN-WT (WT), GFP-OPTN mutant or control (GFP). At 48 h after transfection, total RNA was extracted from these cells and the relative expressions of *TIA1* mRNA to *GAPDH* mRNA were measured by RT-PCR using the corresponding primer sets. The data are presented as the means ± SD (n = 3). *p < 0.05, **p < 0.01, ***p < 0.001.

(D) HeLa cells were transfected with *OPTN-siRNA* (*# 2*). The next day, cells were transfected with the GFP-OPTN-WT (WT), GFP-OPTN mutant, or control (GFP). At 48 h after transfection, cells were exposed to a temperature of 44°C for 30 min and allowed to recover at 37°C for 45-90 min. Cells were immunostained with anti-G3BP1 and anti-TDP-43 antibody. Cells with G3BP1/TDP-43-SG (TDP-43-SG) were counted. The percentage of cells containing TDP-43-SG is displayed as the mean and SD. The data are presented as the means ± SD (n = 5). *p < 0.05. (E and F) HEK293T cells were transfected with *OPTN-siRNA* (*# 2*) or control *siRNA* (*siNT*) with or without *TIA1-siRNA* (# 3). The next day, cells were co-transfected with His-Ub and GFP-TDP-35 plasmid together either with GFP-OPTN-WT (WT), GFP-OPTN mutant or control (GFP) plasmid. At 48 h after transfection, cells were treated with 5 μM MG-132 for 4 h and lysed in 6 M guanidine lysis buffer. His-ubiquitinated proteins were pulled down with Ni-NTA agarose and analyzed by Western blotting with indicated antibodies. The amount of Ub-TDP-35 was measured by densitometry, normalized to that in GFP-transfected OPTN-KD cells, and is shown in (F). The data are presented as the means ± SD (n = 3). *p < 0.05, **p < 0.01, ***p < 0.001 by one-way ANOVA with a Tukey post hoc test. See also Figure S6.

whereas ALS-associated loss-of-function mutations in OPTN induce aberrant SGs that increase the aggregation of ubiquitinated TDP-43 (Figure S7).

Our data showed that the upregulation of TIA1 is a key factor in the increase of ubiquitinated TDP-43 protein and the induction of aberrant SG formation induced by both OPTN-KD and ALS-associated OPTN mutants (Figures 6, 7C, 7D, 8E, and 8F). Notably, TIA1 mutations are also a causative factor of familial ALS with TDP-43 aggregation pathology. *Mackenzie et al.* showed that the overexpression of ALS-associated TIA1 mutants in neuronal cells induced SGs containing TDP-43, and that these TDP-43-SGs showed a delay in SG clearance relative to wild-type TIA1 (Mackenzie et al., 2017). These results suggest that ALS-associated OPTN and TIA1 mutants use a similar mechanism to induce the pathogenic aggregation of TDP-43 in ALS neurons.

OPTN-KD increased the expression of *TIA1* at the mRNA level (Figure 3D). OPTN is known to suppress NF-κB-induced gene transcription (Zhu et al., 2007). However, OPTN repressed the expression of *TIA1* mRNA through a different signaling pathway than NF-κB (Figure 3C). Further studies are needed to elucidate how OPTN inhibits the expression of *TIA1* mRNA.

A previous study showed that the inhibition of autophagy delays SG clearance in heat shock-treated ATG7-KO cells (Buchan et al., 2013). We found that OPTN-KD induced delayed SG clearance in ATG7-KO cells (Figures 3F and 3G). These results suggest that OPTN regulates SG clearance through an autophagy-independent mechanism. Given that OPTN has been shown to activate selective autophagy (Wild et al., 2011), these results suggest that OPTN may have two mechanisms for enhancing SG clearance: the autophagy-independent downregulation of TIA1 and the promotion of autophagy.

At least five of seven ALS-associated OPTN mutants (K59N, A93P, R96L, E478G, and K557T) increased the amounts of ubiquitinated TDP-43 and induced aberrant SGs with delayed SG clearance (Figures 8B and 8D–8F). In addition, all seven ALS-associated OPTN mutants upregulated the expression of TIA1 relative to OPTN-WT (Figure 8C). Mutations in these OPTN mutants are located in the CC1, CC2, UBAN, and ZF domains of OPTN (Figure 8A). Thus, these results suggested that these four domains of OPTN play a role in blocking aberrant SG formation, the reduction of ubiquitinated TDP-43, and the upregulation of TIA1. Further studies are needed to elucidate how ALS-associated OPTN and TIA1 mutants stimulate the formation of TDP-43 inclusion bodies in ALS neurons.

Several studies have shown that TDP-43 aggregation in neurons from ALS patients does not colocalize with some SG-localized proteins, such as TIA1, TIA-1-related protein and fragile X protein (Chen and Cohen, 2019; Mackenzie et al., 2017; Mann et al., 2019). Based on these previous and present findings, the following hypothesis can be considered: after aberrant SG formation, many SG-localized proteins, including TIA1, separate from SGs, but Ub-TDP-43 continues to aggregate, producing Ub-TDP-43 aggregates in ALS neurons, and TIA1 is required for the accumulation of Ub-TDP-43 in SGs but not for the continued aggregation of Ub-TDP-43 after SG clearance.

Limitations of the study

In this study, we found that OPTN decreases the amount of Ub-TDP-43 by downregulating the expression of *TIA1* mRNA. However, it is not known how OPTN downregulates *TIA1* mRNA expression and why some ALS-related OPTN mutants fail to downregulate *TIA1* expression. Elucidation of the mechanisms by which OPTN regulates *TIA1* transcription or mRNA stability in neurons will lead to a better understanding of the pathogenesis of ALS. We found that OPTN-KD increases the amount of TIA1 protein in iPSC-derived neurons. Since motor neurons are predominantly affected in ALS, it will be important to study how OPTN regulates the amount of Ub-TDP-43 in primary motor neurons. Further studies to clarify these points are important to understand the role of OPTN in the motor neuron-specific pathogenesis of ALS.

STAR★METHODS

Detailed methods are provided in the online version of this paper and include the following:

- KEY RESOURCES TABLE
- RESOURCE AVAILABILITY
  - Lead contact

- Material availability
- Data and code availability
- EXPERIMENTAL MODEL AND SUBJECT DETAILS
  - Cell culture
  - Establishment of iPSC-derived neurons
- METHOD DETAILS
  - Plasmids
  - Plasmid transfection
  - RNA interference
  - Western blotting
  - Quantification of ubiquitinated protein
  - Quantification of mRNA
  - Immunofluorescence analyses
- QUANTIFICATION AND STATISTICAL ANALYSIS
  - Quantification of SGs
  - Statistical analysis

SUPPLEMENTAL INFORMATION

Supplemental information can be found online at https://doi.org/10.1016/j.isci.2021.102733.

ACKNOWLEDGMENTS

We would like to thank RIKEN BRC for providing the HeLa cell line and human iPSC, clone1231A3. We would like to thank Dr. Masaaki Komatsu in Juntendo Univ, Japan, for providing the ATG7-KO HeLa cell line. This work was supported by JSPS KAENHI Grant Number (19H03432 to M.F. and 19K17822 and 21K07291 to T.K.)

AUTHOR CONTRIBUTIONS

Conceptualization, T.K. and M.F.; Methodology, T.K. and M.T.; Formal analysis, T.K.; Investigation, T.K.; Resources, T.K., M.T., Y.K. S.Y., J.S., T.K., and O.O.; Writing – Original Draft, T.K. and M.F.; Writing – Review & Editing, T.K., M.T., Y.K. S.Y., J.S., T.K., O.O., and M.F.; Visualization, T.K. and M.F.; Supervision, M.F.; Funding Acquisition, M.F.

DECLARATION OF INTERESTS

The authors declare no conflicts of interest in association with the present study.

Received: September 10, 2020
Revised: April 6, 2021
Accepted: June 14, 2021
Published: July 23, 2021

REFERENCES

Advani, V.M., and Ivanov, P. (2020). Stress granule subtypes: an emerging link to neurodegeneration. Cell Mol. Life Sci. *77*, 4827–4845.

Arai, T., Hasegawa, M., Akiyama, H., Ikeda, K., Nonaka, T., Mori, H., Mann, D., Tsuchiya, K., Yoshida, M., Hashizume, Y., et al. (2006). TDP-43 is a component of ubiquitin-positive tau-negative inclusions in frontotemporal lobar degeneration and amyotrophic lateral sclerosis. Biochem. Biophys. Res. Commun. *351*, 602–611.

Buchan, J.R., Kolaitis, R.M., Taylor, J.P., and Parker, R. (2013). Eukaryotic stress granules are cleared by autophagy and Cdc48/VCP function. Cell *153*, 1461–1474.

Chen, Y., and Cohen, T.J. (2019). Aggregation of the nucleic acid-binding protein TDP-43 occurs via distinct routes that are coordinated with stress granule formation. J. Biol. Chem. *294*, 3696–3706.

Chernyshova, K., Inoue, K., Yamashita, S.I., Fukuchi, T., and Kanki, T. (2019). Glaucoma-associated mutations in the optineurin gene have limited impact on parkin-dependent mitophagy. Invest. Ophthalmol. Vis. Sci. *60*, 3625–3635.

Corbet, G.A., and Parker, R. (2020). RNP granule formation: lessons from P-bodies and stress granules. Cold Spring Harb Symp. Quant Biol. *84*, 203–215.

Ganassi, M., Mateju, D., Bigi, I., Mediani, L., Poser, I., Lee, H.O., Seguin, S.J., Morelli, F.F., Vinet, J., Leo, G., et al. (2016). A surveillance function of the HSPB8-BAG3-HSP70 chaperone complex ensures stress granule integrity and dynamism. Mol. Cell *63*, 796–810.

Higashi, S., Kabuta, T., Nagai, Y., Tsuchiya, Y., Akiyama, H., and Wada, K. (2013). TDP-43 associates with stalled ribosomes and contributes to cell survival during cellular stress. J. Neurochem. *126*, 288–300.

Hofweber, M., Hutten, S., Bourgeois, B., Spreitzer, E., Niedner-Boblenz, A., Schifferer, M., Ruepp, M.D., Simons, M., Niessing, D., Madl, T., et al. (2018). Phase separation of FUS is suppressed by its nuclear import receptor and arginine methylation. Cell *173*, 706–719.e13.

Ito, D., Hatano, M., and Suzuki, N. (2017). RNA binding proteins and the pathological cascade in

ALS/FTD neurodegeneration. Sci. Transl. Med. *9*, eaah5436.

Kedersha, N.L., Gupta, M., Li, W., Miller, I., and Anderson, P. (1999). RNA-binding proteins TIA-1 and TIAR link the phosphorylation of eIF-2 alpha to the assembly of mammalian stress granules. J. Cell Biol. *147*, 1431–1442.

Li, Q., Yokoshi, M., Okada, H., and Kawahara, Y. (2015). The cleavage pattern of TDP-43 determines its rate of clearance and cytotoxicity. Nat. Commun. *6*, 6183.

Li, Y.R., King, O.D., Shorter, J., and Gitler, A.D. (2013). Stress granules as crucibles of ALS pathogenesis. J. Cell Biol. *201*, 361–372.

Mackenzie, I.R., Nicholson, A.M., Sarkar, M., Messing, J., Purice, M.D., Pottier, C., Annu, K., Baker, M., Perkerson, R.B., Kurti, A., et al. (2017). TIA1 mutations in amyotrophic lateral sclerosis and frontotemporal dementia promote phase separation and alter stress granule dynamics. Neuron *95*, 808–816.e9.

Maharana, S., Wang, J., Papadopoulos, D.K., Richter, D., Pozniakovsky, A., Poser, I., Bickle, M., Rizk, S., Guillen-Boixet, J., Franzmann, T.M., et al. (2018). RNA buffers the phase separation behavior of prion-like RNA binding proteins. Science *360*, 918–921.

Mann, J.R., Gleixner, A.M., Mauna, J.C., Gomes, E., DeChellis-Marks, M.R., Needham, P.G., Copley, K.E., Hurtle, B., Portz, B., Pyles, N.J., et al. (2019). RNA binding antagonizes neurotoxic phase transitions of TDP-43. Neuron *102*, 321–338.e8.

Markovinovic, A., Cimbro, R., Ljutic, T., Kriz, J., Rogelj, B., and Munitic, I. (2017). Optineurin in amyotrophic lateral sclerosis: multifunctional adaptor protein at the crossroads of different neuroprotective mechanisms. Prog. Neurobiol. *154*, 1–20.

Maruyama, H., Morino, H., Ito, H., Izumi, Y., Kato, H., Watanabe, Y., Kinoshita, Y., Kamada, M., Nodera, H., Suzuki, H., et al. (2010). Mutations of optineurin in amyotrophic lateral sclerosis. Nature *465*, 223–226.

Masrori, P., and Van Damme, P. (2020). Amyotrophic lateral sclerosis: a clinical review. Eur. J. Neurol. *10*, 1918–1929.

Mateju, D., Franzmann, T.M., Patel, A., Kopach, A., Boczek, E.E., Maharana, S., Lee, H.O., Carra, S., Hyman, A.A., and Alberti, S. (2017). An aberrant phase transition of stress granules triggered by misfolded protein and prevented by chaperone function. EMBO J. *36*, 1669–1687.

McGurk, L., Gomes, E., Guo, L., Mojsilovic-Petrovic, J., Tran, V., Kalb, R.G., Shorter, J., and Bonini, N.M. (2018). Poly(ADP-Ribose) prevents pathological phase separation of TDP-43 by promoting liquid demixing and stress granule localization. Mol. Cell *71*, 703–717.e9.

McQuin, C., Goodman, A., Chernyshev, V., Kamentsky, L., Cimini, B.A., Karhohs, K.W., Doan, M., Ding, L., Rafelski, S.M., Thirstrup, D., et al. (2018). CellProfiler 3.0: next-generation image processing for biology. PLoS Biol. *16*, e2005970.

Molliex, A., Temirov, J., Lee, J., Coughlin, M., Kanagaraj, A.P., Kim, H.J., Mittag, T., and Taylor, J.P. (2015). Phase separation by low complexity domains promotes stress granule assembly and drives pathological fibrillization. Cell *163*, 123–133.

Nakagawa, M., Taniguchi, Y., Senda, S., Takizawa, N., Ichisaka, T., Asano, K., Morizane, A., Doi, D., Takahashi, J., Nishizawa, M., et al. (2014). A novel efficient feeder-free culture system for the derivation of human induced pluripotent stem cells. Sci Rep *4*, 3594.

Nakazawa, S., Oikawa, D., Ishii, R., Ayaki, T., Takahashi, H., Takeda, H., Ishitani, R., Kamei, K., Takeyoshi, I., Kawakami, H., et al. (2016). Linear ubiquitination is involved in the pathogenesis of optineurin-associated amyotrophic lateral sclerosis. Nat. Commun. *7*, 12547.

Neumann, M., Sampathu, D.M., Kwong, L.K., Truax, A.C., Micsenyi, M.C., Chou, T.T., Bruce, J., Schuck, T., Grossman, M., Clark, C.M., et al. (2006). Ubiquitinated TDP-43 in frontotemporal lobar degeneration and amyotrophic lateral sclerosis. Science *314*, 130–133.

Schindelin, J., Arganda-Carreras, I., Frise, E., Kaynig, V., Longair, M., Pietzsch, T., Preibisch, S., Rueden, C., Saalfeld, S., Schmid, B., et al. (2012). Fiji: an open-source platform for biological-image analysis. Nat Methods *9*, 676–682.

Soeda, S., Saito, R., Fujita, N., Fukuta, K., and Taniura, H. (2019). Neuronal differentiation defects in induced pluripotent stem cells derived from a Prader-Willi syndrome patient. Neurosci. Lett. *703*, 162–167.

Sreedharan, J., Blair, I.P., Tripathi, V.B., Hu, X., Vance, C., Rogelj, B., Ackerley, S., Durnall, J.C., Williams, K.L., Buratti, E., et al. (2008). TDP-43 mutations in familial and sporadic amyotrophic lateral sclerosis. Science *319*, 1668–1672.

Suk, T.R., and Rousseaux, M.W.C. (2020). The role of TDP-43 mislocalization in amyotrophic lateral sclerosis. Mol. Neurodegener. *15*, 45.

Takahashi, M., Kitaura, H., Kakita, A., Kakihana, T., Katsuragi, Y., Nameta, M., Zhang, L., Iwakura, Y., Nawa, H., Higuchi, M., et al. (2018). USP10 is a driver of ubiquitinated protein aggregation and aggresome formation to inhibit apoptosis. Iscience *9*, 433.

Verdile, V., De Paola, E., and Paronetto, M.P. (2019). Aberrant phase transitions: side effects and novel therapeutic strategies in human disease. Front. Genet. *10*, 173.

Wang, B., Maxwell, B.A., Joo, J.H., Gwon, Y., Messing, J., Mishra, A., Shaw, T.I., Ward, A.L., Quan, H., Sakurada, S.M., et al. (2019). ULK1 and ULK2 regulate stress granule disassembly through phosphorylation and activation of VCP/p97. Mol. Cell *74*, 742–757.e8.

Wild, P., Farhan, H., McEwan, D.G., Wagner, S., Rogov, V.V., Brady, N.R., Richter, B., Korac, J., Waidmann, O., Choudhary, C., et al. (2011). Phosphorylation of the autophagy receptor optineurin restricts Salmonella growth. Science *333*, 228–233.

Wils, H., Kleinberger, G., Janssens, J., Pereson, S., Joris, G., Cuijt, I., Smits, V., Ceuterick-de Groote, C., Van Broeckhoven, C., and Kumar-Singh, S. (2010). TDP-43 transgenic mice develop spastic paralysis and neuronal inclusions characteristic of ALS and frontotemporal lobar degeneration. Proc. Natl. Acad. Sci. U S A *107*, 3858–3863.

Wong, Y.C., and Holzbaur, E.L. (2014). Optineurin is an autophagy receptor for damaged mitochondria in parkin-mediated mitophagy that is disrupted by an ALS-linked mutation. Proc. Natl. Acad. Sci. U S A *111*, E4439–E4448.

Xiao, S., Sanelli, T., Chiang, H., Sun, Y., Chakrabartty, A., Keith, J., Rogaeva, E., Zinman, L., and Robertson, J. (2015). Low molecular weight species of TDP-43 generated by abnormal splicing form inclusions in amyotrophic lateral sclerosis and result in motor neuron death. Acta Neuropathol. *130*, 49–61.

Yokoseki, A., Shiga, A., Tan, C.F., Tagawa, A., Kaneko, H., Koyama, A., Eguchi, H., Tsujino, A., Ikeuchi, T., Kakita, A., et al. (2008). TDP-43 mutation in familial amyotrophic lateral sclerosis. Ann. Neurol. *63*, 538–542.

Zhang, Y.J., Xu, Y.F., Cook, C., Gendron, T.F., Roettges, P., Link, C.D., Lin, W.L., Tong, J., Castanedes-Casey, M., Ash, P., et al. (2009). Aberrant cleavage of TDP-43 enhances aggregation and cellular toxicity. Proc. Natl. Acad. Sci. U S A *106*, 7607–7612.

Zhu, G., Wu, C.J., Zhao, Y., and Ashwell, J.D. (2007). Optineurin negatively regulates TNFalpha- induced NF-kappaB activation by competing with NEMO for ubiquitinated RIP. Curr. Biol. *17*, 1438–1443.

STAR★METHODS

KEY RESOURCES TABLE

REAGENT or RESOURCE	SOURCE	IDENTIFIER
Antibodies		
OPTN	Santa Cruz Biotechnology	Cat# sc-166576; RRID: AB_2156554
OPTN	Thermo Fisher	Cat# PA5-28249; RRID: AB_2545725
TIA1	Abcam	Cat# ab40693; RRID: AB_2201438
USP10	Sigma-Aldrich	Cat# HPA006731; RRID: AB_1080495
TDP-43	Proteintech	Cat# 12892-1-AP; RRID: AB_2200505
ubiquitin	Santa Cruz Biotechnology	Cat# sc-8017 AC; RRID: AB_2762364
ubiquitin	Abcam	Cat# ab7780; RRID: AB_306069
p62	MBL International	Cat# PM045; RRID: AB_1279301
G3BP1	BD Transduction Laboratories	Cat# 611127; RRID: AB_398438
PABP	Abcam	Cat# ab21060; RRID: AB_777008
GFP	Santa Cruz Biotechnology	Cat# sc-9996; RRID: AB_627695
LC3	MBL International	Cat# PM036; RRID: AB_2274121
β-actin	Santa Cruz Biotechnology	Cat# sc-47778; RRID: AB_626632
MAP-2	Santa Cruz Biotechnology	Cat# sc-74421; RRID: AB_1126215
LAMP1	Santa Cruz Biotechnology	Cat# sc-20011; RRID: AB_626853
Alexa Fluor® 405-conjugated anti-mouse	Abcam	Cat# ab175658; RRID: AB_2687445
Alexa Fluor® 488-conjugated anti-mouse	Thermo Fisher	Cat# A-21202, RRID: AB_141607
Alexa Fluor® 488-conjugated anti-rabbit	Thermo Fisher	Cat# A-21206; RRID: AB_2535792
Alexa Fluor® 594-conjugated anti-rabbit	Thermo Fisher	Cat# A-21207; RRID: AB_141637
anti-rabbit IgG-HRP	Santa Cruz Biotechnology	Cat# sc-2357, RRID: AB_628497
anti-goat IgG-HRP	Santa Cruz Biotechnology	Cat# sc-2354; RRID: AB_628490
anti-mouse IgG-HRP	Bio-Rad	Cat# 170-6516; RRID: AB_11125547
Bacterial and virus strains		
NEB 5-alpha Competent E. coli	NEB	C2987H
Chemicals, peptides, and recombinant proteins		
MG-132	Calbiochem	474790
bafilomycin A1	Sigma-Aldrich	B1793
puromycin	Sigma-Aldrich	P8833
BAY 11-7082	TCI Chemicals	T2846
Hoechst 33258	Molecular Probes	H-3569
Ni-NTA Agarose	QIAGEN	30230
Guanidine-HCl	Wako	074-05005
Can Get Signal immunoreaction Enhancer Solution	TOYOBO	NKB-101
ECL Western Blotting Detection Reagents	GE Healthcare	RPN2209
Experimental models: Cell lines		
HeLa	RIKEN BRC	RCB0007
HEK293T	Takahashi et al., 2018	N/A
Neuro-2a	Takahashi et al., 2018	N/A
ATG7-KO HeLa	A kind gift from Dr. Komatsu, Juntendo Univ, Japan	N/A
Human iPS	RIKEN BRC	1231A3

(*Continued on next page*)

Continued

REAGENT or RESOURCE	SOURCE	IDENTIFIER
Oligonucleotides		
siOPTN # 1	Thermo Fisher	OPTNHSS115415
siOPTN # 2	Thermo Fisher	OPTNHSS115416
siOPTN # 3	Thermo Fisher	OPTNHSS173415
mouse siOptn # 1	Thermo Fisher	OptnMSS230850
mouse siOptn # 2	Thermo Fisher	OptnMSS230851
siTIA1 # 1	QIAGEN	SI00133105
siTIA1 # 3	QIAGEN	SI00301917
Recombinant DNA		
pMXs-GFP	Cell Biolabs, Inc	RTV-010
pMXs-GFP-OPTN	This paper	N/A
pFLAG-G3BP1	Takahashi et al., 2018	N/A
pFLAG-TIA1	A kind gift from Dr. Ravindra Singh, Iowa State Univ., IA, USA	N/A
pEGFP-C3	TAKARA	Discontinued
pEGFP-TIA1	A kind gift from Dr. J. Paul Taylor, St. Jude Children's Research Hospital, TN, USA	N/A
GFP-TDP-35	This paper	N/A
Software and algorithms		
ImageJ (Fiji)	NIH, Schindelin et al., 2012	RRID:SCR_003070
CellProfiler	The Broad Institute of Harvard and MIT, McQuin et al., 2018	RRID:SCR_007358
RStudio	https://rstudio.com/	RRID:SCR_000432
Other		
Fluorescence microscope	KEYENCE	BZ-X810

RESOURCE AVAILABILITY

Lead contact

Further information and requests for reagents may be directed to and will be fulfilled by the Lead Contact, Masahiro Fujii (fujiimas@med.niigata-u.ac.jp).

Material availability

Materials generated in this study will be made available upon reasonable request and may require a material transfer agreement.

Data and code availability

All data supporting findings of this work are provided within the manuscript and its supplemental information section.

EXPERIMENTAL MODEL AND SUBJECT DETAILS

Cell culture

HeLa and HEK293T cells were cultured in Dulbecco's modified Eagle's medium (DMEM) supplemented with 10% heat-inactivated fetal bovine serum (FBS), 4 mM L-glutamine, 50 units/ml penicillin, 50 μg/mL streptomycin, and MEM non-essential amino acid (MEM-NEAA) (Thermo Fisher Scientific) (10% FBS/DMEM). Neuro-2a is a mouse neuroblastoma cell line and the cells were cultured as previously described (Takahashi et al., 2018). Gene knockout (KO) HeLa cells (OPTN-KO) were established by the CRISPER-Cas9 method, as described previously (Chernyshova et al., 2019).

Establishment of iPSC-derived neurons

Human induced pluripotent stem cells (iPSCs) (clone1231A3) (Nakagawa et al., 2014) were obtained from Riken BioResource Research Center (BRC). iPSCs were cultured under the conditions of the feeder-free method established by the Center for iPS Cell Research and Application (CiRA), Kyoto University. In brief, iPSCs were seeded onto 6-well plates coated with Laminin-511 E8 protein (Laminin+ 6-well plate) and cultured in iPSC medium (StemFit AK02N; AJINOMOTO). Laminin-511 E8 is a recombinant protein of the E8 fragment of Laminin-511 that supports the adhesion and expansion of iPSCs. StemFit AK02N is medium for maintaining iPSCs under feeder-free conditions. After the cell density reached confluence following at least 1 passage, cells were seeded at 1×10^5/well in the Laminin+ 6-well plate. The next day, the cells were cultured in PSC Neural Induction Medium (Thermo Fisher) to induce differentiation into neural stem cells (NSCs) and cultured for 1 week. The cells were then passaged in StemPro NSC SFM medium (Thermo Fisher) at 2×10^5/well in a Matrigel-coated 6-well plate. On day 2 after passage, the cells were cultured in 2% B27/neurobasal medium to induce differentiation into neurons. On day 9 after culture, the cells were passaged on Matrigel-coated coverslips in 24-well plate. Two days later, cells were transfected with 5 pmol of *siRNA* using Lipofectamine RNAiMAX. At 24 h after transfection, the medium was changed. At 72 h post-transfection, the cells were used for experiments.

METHOD DETAILS

Plasmids

pMXs-neo-GFP is a retroviral vector that produces a GFP fusion protein. pMXs-neo-GFP-OPTN was generated by inserting human OPTN cDNA in pMXs-neo-GFP as described previously (Chernyshova et al., 2019). OPTN cDNA resistant to three *OPTN-siRNA*s (*# 1* to *# 3*) was generated by the following method. An OPTN cDNA fragment (824-1133 bp) containing three synonymous DNA mutations to the three *OPTN-siRNA* target sequences (*siOPTN #1-#3*) was synthesized by the Invitrogen GeneArt service (Thermo Fisher). This mutated OPTN cDNA fragment was replaced with the wild-type OPTN cDNA fragment of pMXs-neo-GFP-OPTN using an In-Fusion cloning kit (TAKARA). The siRNA-resistant OPTN mutant genes (K59N, A93P, R96L, V295F, E478G, R545Q and K557T) were also prepared using a mutagenesis kit (PrimeSTAR Mutagenesis Basal Kit; TAKARA). pGFP-TDP-35 is an expression plasmid of a fusion protein of TDP-35 and N-terminal GFP. pMT107 (called His-Ub in this study) is a 6 histidine-tagged ubiquitin expression plasmid, provided by Dr. Mathias Treier (MDC Berlin, Germany).

Plasmid transfection

Plasmids were transfected into HeLa or HEK293T cells in a 6-well plate (Corning) using FuGENE 6 (Promega) or Lipofectamine 2000 (Invitrogen) reagents according to the manufacturer's instructions.

RNA interference

Human or mouse *OPTN*-specific small interfering RNA (siRNA) (Oligo ID: HSS113116, HSS113117) was purchased from Invitrogen. Human *TIA1-siRNA* (SI00133105, SI03119452 (FlexiTube siRNA) or control siRNA (Cat. No. 1027280) was purchased from QIAGEN. These siRNAs (50 pmol for *OPTN-siRNA* and 20 pmol for *TIA1-siRNA*) were transfected into cells using Lipofectamine RNAiMAX according to the manufacturer's protocol (Invitrogen).

Western blotting

Cells were lysed with SDS lysis buffer. Cell lysates (10 μg of proteins) were separated by SDS-PAGE, electrophoretically transferred to a PVDF membrane (Immobilon; Millipore) and incubated with Blocking One (Nacalai) and the indicated antibodies diluted with Can Get Signal buffer (TOYOBO). Immunoreactive bands were detected with an enhanced chemiluminescence (ECL) detection system (ECL Western Blotting Detection Reagents; GE Healthcare, Pierce™ ECL Plus Western Blotting Substrate; Thermo Fisher Scientific) and visualized with Amersham Hyperfilm ECL film (Amersham).

Quantification of ubiquitinated protein

HEK293T cells (2×10^5) were seeded in a 60-mm dish (Corning) and cells were transfected with *OPTN-siRNA* or control (*NT*). The next day, cells were further transfected with six-His-ubiquitin (His-Ub) and GFP-TDP-35 plasmid. At 48 h after plasmid transfection, cells were lysed with buffer A (6 M guanidine-HCl, 0.1 M Na_2HPO_4, 0.1 M NaH_2PO_4, 10 mM imidazole, pH 8.0) and sonicated. Lysates after centrifugation were incubated with Ni-NTA-agarose (QIAGEN) at room temperature for 3 h. After centrifugation, the pellet was

washed 3 times with buffer A, twice with mixture of buffer A and buffer B (1:4), and twice with buffer B (25 mM Tris-HCl pH 6.8, 20 mM imidazole). The proteins bound to Ni-NTA agarose were then eluted by SDS-lysis buffer (4% SDS, 10% sucrose and 125 mM Tris, pH 6.8) containing 200 mM imidazole. The eluted proteins were subjected to Western blotting. The amount of bands of Ub-GFP-TDP-35 was measured by densitometry.

Quantification of mRNA

Total RNA was extracted from HEK293T cells using an RNA extraction kit (NucleoSpin RNA®, TAKARA) according to the manufacturer's protocol. The total RNA (10 ng) was used in the RT-PCR reaction using a One Step TB Green™ PrimeScript™ RT-PCR Kit II (TAKARA) and a primer set. Real-time PCR was performed using a Thermal Cycler Dice® Real Time System (TAKARA). The *TIA1* mRNA level was normalized according to the *β-actin or GAPDH* mRNA level.

Immunofluorescence analyses

Cells were cultured on coverslips in a 6-well plate, fixed with 4% paraformaldehyde in phosphate buffered saline (PBS) and permeabilized by 0.1% Triton X-100 in PBS (Triton/PBS). Cells were treated with 0.1% Triton/PBS containing 0.2% gelatin, incubated with primary (anti-G3BP1, anti-TIA1 or anti-ubiquitin) antibodies and then with secondary antibodies. Cell nuclei were stained with Hoechst 33258. The samples were then mounted with ProLong Glass antifade mounting reagent (Thermo Fisher). Immunofluorescence images of cells were acquired with a fluorescence microscope (BZ-X810; KEYENCE) and analyzed using the FIJI ImageJ software program (https://imagej.net) or CellProfiler software program (https://cellprofiler.org).

QUANTIFICATION AND STATISTICAL ANALYSIS

Quantification of SGs

Immunofluorescence images of cells were analyzed using the FIJI ImageJ software program (https://imagej.net) or CellProfiler software program (https://cellprofiler.org). G3BP1-positive or TIA1-positive aggregates exceeding 0.1 μm^2 in size were evaluated as SGs. TDP-43-positive and Ub-positive aggregates exceeding 0.2 μm^2 in size were evaluated as TDP-43-aggregates and Ub-aggregates, respectively. TDP-43-positive and Ub-positive aggregates that colocalized with SGs were evaluated as TDP-43-SGs and Ub-SGs, respectively. Cells with one or more TDP-43-SG were counted as cells with TDP-43-SG. Over 100 cells in random fields were analyzed to determine the number of cells containing SGs or the size of SGs. The percentage of cells with SGs was calculated as the ratio of SG-positive cells to total cells. The detailed methods used to measure the size of SGs with the FIJI ImageJ (Schindelin et al., 2012) or CellProfiler software program have been described previously (Hofweber et al., 2018; McQuin et al., 2018).

Statistical analysis

Quantitative data were analyzed by a one-way ANOVA with a Tukey post hoc test to determine the statistical significance of differences using the R Studio software program.